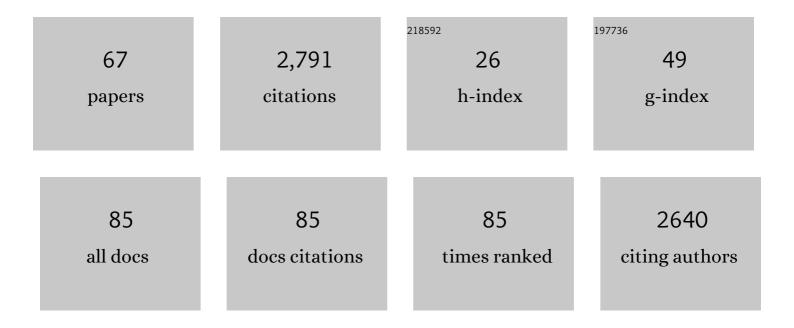
Eric M Pierce

List of Publications by Year in descending order

Source: https://exaly.com/author-pdf/4765844/publications.pdf Version: 2024-02-01



#	Article	IF	CITATIONS
1	Competitive exchange between divalent metal ions [Cu(II), Zn(II), Ca(II)] and Hg(II) bound to thiols and natural organic matter. Journal of Hazardous Materials, 2022, 424, 127388.	6.5	2
2	Unravelling biogeochemical drivers of methylmercury production in an Arctic fen soil and a bog soil. Environmental Pollution, 2022, 299, 118878.	3.7	8
3	Machine learning–based observation-constrained projections reveal elevated global socioeconomic risks from wildfire. Nature Communications, 2022, 13, 1250.	5.8	19
4	From legacy contamination to watershed systems science: a review of scientific insights and technologies developed through DOE-supported research in water and energy security. Environmental Research Letters, 2022, 17, 043004.	2.2	12
5	Isotope exchange between mercuric [Hg(II)] chloride and Hg(II) bound to minerals and thiolate ligands: Implications for enriched isotope tracer studies. Geochimica Et Cosmochimica Acta, 2021, 292, 468-481.	1.6	17
6	Dissolution kinetics of a sodium borosilicate glass in Tris buffer solutions: impact of Tris concentration and acid (HCl/HNO ₃) identity. Physical Chemistry Chemical Physics, 2021, 23, 16165-16179.	1.3	7
7	Bedrock architecture, soil texture, and hyporheic zone characterization combining electrical resistivity and induced polarization imaging. Journal of Applied Geophysics, 2021, 188, 104306.	0.9	17
8	Spectroscopic and computational investigations of organometallic complexation of group 12 transition metals by methanobactins from Methylocystis sp. SB2. Journal of Inorganic Biochemistry, 2021, 223, 111496.	1.5	2
9	An insight into the corrosion of alkali aluminoborosilicate glasses in acidic environments. Physical Chemistry Chemical Physics, 2020, 22, 1881-1896.	1.3	35
10	Rates and Dynamics of Mercury Isotope Exchange between Dissolved Elemental Hg(0) and Hg(II) Bound to Organic and Inorganic Ligands. Environmental Science & Technology, 2020, 54, 15534-15545.	4.6	17
11	Energetics of Salt-Bearing Sodalites, Na ₈ Al ₆ Si ₆ O ₂₄ X ₂ (X = SO ₄ ,) Tj Earth and Space Chemistry, 2020, 4, 2153-2161.	ETQq1 1 0.	784314 rgB1
12	Dissolved organic matter reduces the effectiveness of sorbents for mercury removal. Science of the Total Environment, 2019, 690, 410-416.	3.9	42
13	Mercury Sorption and Desorption on Organo-Mineral Particulates as a Source for Microbial Methylation. Environmental Science & Technology, 2019, 53, 2426-2433.	4.6	52
14	Influence of young cement water on the corrosion of the International Simple Glass. Npj Materials Degradation, 2019, 3, .	2.6	22
15	Mercury Adsorption on Minerals and Its Effect on Microbial Methylation. ACS Earth and Space Chemistry, 2019, 3, 1338-1345.	1.2	18
16	Soil Aggregate Microbial Communities: Towards Understanding Microbiome Interactions at Biologically Relevant Scales. Applied and Environmental Microbiology, 2019, 85, .	1.4	233
17	Mercury Uptake by <i>Desulfovibrio desulfuricans</i> ND132: Passive or Active?. Environmental Science & Technology, 2019, 53, 6264-6272.	4.6	33
18	Characterization of iron oxide nanoparticle films at the air–water interface in Arctic tundra waters. Science of the Total Environment, 2018, 633, 1460-1468.	3.9	8

ERIC M PIERCE

#	Article	IF	CITATIONS
19	Toward an understanding of surface layer formation, growth, and transformation at the glass–fluid interface. Geochimica Et Cosmochimica Acta, 2018, 229, 65-84.	1.6	19
20	Influence of Structural Defects on Biomineralized ZnS Nanoparticle Dissolution: An in-Situ Electron Microscopy Study. Environmental Science & Technology, 2018, 52, 1139-1149.	4.6	42
21	Understanding the structural drivers governing glass–water interactions in borosilicate based model bioactive glasses. Acta Biomaterialia, 2018, 65, 436-449.	4.1	43
22	Removal of inorganic mercury by selective extraction and coprecipitation for determination of methylmercury in mercury-contaminated soils by chemical vapor generation inductively coupled plasma mass spectrometry (CVG-ICP-MS). Analytica Chimica Acta, 2018, 1041, 68-77.	2.6	35
23	Nanomolar Copper Enhances Mercury Methylation by <i>Desulfovibrio desulfuricans</i> ND132. Environmental Science and Technology Letters, 2018, 5, 372-376.	3.9	24
24	Improved ZnS nanoparticle properties through sequential NanoFermentation. Applied Microbiology and Biotechnology, 2018, 102, 8329-8339.	1.7	2
25	Quantitative Proteomic Analysis of Biological Processes and Responses of the Bacterium <i>Desulfovibrio desulfuricans</i> ND132 upon Deletion of Its Mercury Methylation Genes. Proteomics, 2018, 18, e1700479.	1.3	22
26	Low temperature heat capacity and thermodynamic functions of anion bearing sodalites Na8Al6Si6O24X2 (X = SO4, ReO4, Cl, I). Journal of Chemical Thermodynamics, 2017, 114, 14-24.	1.0	8
27	Structure and Thermochemistry of Perrhenate Sodalite and Mixed Guest Perrhenate/Pertechnetate Sodalite. Environmental Science & Technology, 2017, 51, 997-1006.	4.6	19
28	Modelling the sulfate capacity of simulated radioactive waste borosilicate glasses. Journal of Alloys and Compounds, 2017, 695, 656-667.	2.8	31
29	Contrasting Effects of Dissolved Organic Matter on Mercury Methylation by <i>Geobacter sulfurreducens</i> PCA and <i>Desulfovibrio desulfuricans</i> ND132. Environmental Science & Technology, 2017, 51, 10468-10475.	4.6	74
30	Glass–water interaction: Effect of high-valence cations on glass structure and chemical durability. Geochimica Et Cosmochimica Acta, 2016, 181, 54-71.	1.6	36
31	Anaerobic Mercury Methylation and Demethylation by <i>Geobacter bemidjiensis</i> Bem. Environmental Science & Technology, 2016, 50, 4366-4373.	4.6	121
32	Response to Comment on "Anaerobic Mercury Methylation and Demethylation by Geobacter Bemidjiensis Bem― Environmental Science & Technology, 2016, 50, 9800-9801.	4.6	2
33	Effects of Cellular Sorption on Mercury Bioavailability and Methylmercury Production by <i>Desulfovibrio desulfuricans</i> ND132. Environmental Science & Technology, 2016, 50, 13335-13341.	4.6	78
34	Evidence of technetium and iodine release from a sodalite-bearing ceramic waste form. Applied Geochemistry, 2016, 66, 210-218.	1.4	11
35	Mineral assemblage transformation of a metakaolin-based waste form after geopolymer encapsulation. Journal of Nuclear Materials, 2016, 473, 320-332.	1.3	13
36	Mercury-Pollution Induction of Intracellular Lipid Accumulation and Lysosomal Compartment Amplification in the Benthic Foraminifer Ammonia parkinsoniana. PLoS ONE, 2016, 11, e0162401.	1.1	17

ERIC M PIERCE

#	Article	IF	CITATIONS
37	Monte Carlo simulations of coupled diffusion and surface reactions during the aqueous corrosion of borosilicate glasses. Journal of Non-Crystalline Solids, 2015, 408, 142-149.	1.5	18
38	Immobilization and exchange of perrhenate in sodalite and cancrinite. Microporous and Mesoporous Materials, 2015, 214, 115-120.	2.2	22
39	Perrhenate incorporation into binary mixed sodalites: The role of anion size and implications for technetium-99 sequestration. Chemical Geology, 2015, 395, 138-143.	1.4	41
40	In situ remediation technologies for mercury-contaminated soil. Environmental Science and Pollution Research, 2015, 22, 8124-8147.	2.7	102
41	Formation of Soluble Mercury Oxide Coatings: Transformation of Elemental Mercury in Soils. Environmental Science & Technology, 2015, 49, 12105-12111.	4.6	17
42	Mercury source zone identification using soil vapor sampling and analysis. Frontiers of Environmental Science and Engineering, 2015, 9, 596-604.	3.3	2
43	Topography and Mechanical Property Mapping of International Simple Glass Surfaces with Atomic Force Microscopy. , 2014, 7, 216-222.		23
44	Modeling Interfacial Glassâ€Water Reactions: Recent Advances and Current Limitations. International Journal of Applied Glass Science, 2014, 5, 421-435.	1.0	34
45	Performance of the Fluidized Bed Steam Reforming product under hydraulically unsaturated conditions. Journal of Environmental Radioactivity, 2014, 131, 119-128.	0.9	10
46	Competitive Incorporation of Perrhenate and Nitrate into Sodalite. Environmental Science & Technology, 2014, 48, 12851-12857.	4.6	66
47	Experimental determination of the speciation, partitioning, and release of perrhenate as a chemical surrogate for pertechnetate from a sodalite-bearing multiphase ceramic waste form. Applied Geochemistry, 2014, 42, 47-59.	1.4	20
48	Monte Carlo simulations of the corrosion of aluminoborosilicate glasses. Journal of Non-Crystalline Solids, 2013, 378, 273-281.	1.5	26
49	An international initiative on long-term behavior of high-level nuclear waste glass. Materials Today, 2013, 16, 243-248.	8.3	417
50	Characterization of soils from an industrial complex contaminated with elemental mercury. Environmental Research, 2013, 125, 20-29.	3.7	54
51	Rapid Removal of Hg(II) from Aqueous Solutions Using Thiol-Functionalized Zn-Doped Biomagnetite Particles. ACS Applied Materials & Interfaces, 2012, 4, 4373-4379.	4.0	96
52	Monte Carlo simulations of the dissolution of borosilicate glasses in near-equilibrium conditions. Journal of Non-Crystalline Solids, 2012, 358, 1324-1332.	1.5	20
53	Diffusive release of uranium from contaminated sediments into capillary fringe pore water. Journal of Contaminant Hydrology, 2012, 140-141, 164-172.	1.6	4
54	Monte Carlo simulations of the dissolution of borosilicate and aluminoborosilicate glasses in dilute aqueous solutions. Geochimica Et Cosmochimica Acta, 2011, 75, 5296-5309.	1.6	25

ERIC M PIERCE

#	Article	IF	CITATIONS
55	Deep-UV Raman spectroscopic analysis of structure and dissolution rates of silica-rich sodium borosilicate glasses. Journal of Non-Crystalline Solids, 2011, 357, 2170-2177.	1.5	24
56	Development of long-term behavior models for radioactive waste forms. , 2011, , 433-454.		3
57	Combined Experimental and Computational Approach to Predict the Glass-Water Reaction. Nuclear Technology, 2011, 176, 22-39.	0.7	9
58	Experimental determination of the effect of the ratio of B/Al on glass dissolution along the nepheline (NaAlSiO4)–malinkoite (NaBSiO4) join. Geochimica Et Cosmochimica Acta, 2010, 74, 2634-2654.	1.6	85
59	Aluminoborosilicate waste glass dissolution under alkaline conditions at 40°C: implications for a chemical affinity-based rate equation. Environmental Chemistry, 2008, 5, 73.	0.7	24
60	An experimental study of the dissolution rates of simulated aluminoborosilicate waste glasses as a function of pH and temperature under dilute conditions. Applied Geochemistry, 2008, 23, 2559-2573.	1.4	75
61	Experimentally determined dissolution kinetics of Na-rich borosilicate glass at far from equilibrium conditions: Implications for Transition State Theory. Geochimica Et Cosmochimica Acta, 2008, 72, 2767-2788.	1.6	59
62	Sequestration and retention of uranium(VI) in the presence of hydroxylapatite under dynamic geochemical conditions. Environmental Chemistry, 2008, 5, 40.	0.7	34
63	Accelerated weathering of high-level and plutonium-bearing lanthanide borosilicate waste glasses under hydraulically unsaturated conditions. Applied Geochemistry, 2007, 22, 1841-1859.	1.4	51
64	Experimental determination of the dissolution kinetics of zero-valent iron in the presence of organic complexants. Environmental Chemistry, 2007, 4, 260.	0.7	26
65	Efficacy of soluble sodium tripolyphosphate amendments for the in-situ immobilisation of uranium. Environmental Chemistry, 2007, 4, 293.	0.7	15
66	The Accelerated Weathering of a Radioactive Low-Activity Waste Glass under Hydraulically Unsaturated Conditions: Experimental Results from a Pressurized Unsaturated Flow Test. Nuclear Technology, 2006, 155, 149-165.	0.7	31
67	Experimental determination of UO2(cr) dissolution kinetics: Effects of solution saturation state and pH. Journal of Nuclear Materials, 2005, 345, 206-218.	1.3	68